Modal Interferometer Based on a C-Shaped Ultrathin Fiber Taper for High-Sensitivity Refractive Index Measurement

Applied Physics Express **5** (2012) 012502
DOI: 10.1143/APEX.5.012502

Modal Interferometer Based on a C-Shaped Ultrathin Fiber Taper for High-Sensitivity Refractive Index Measurement

Haimei Luo[1,2], Xinwan Li[1]*, Weiwen Zou[1], Wenning Jiang[1], and Jianping Chen[1]

[1]*State Key Laboratory of Advanced Optical Communication Systems and Networks, Department of Electronic Engineering, Shanghai Jiao Tong University, Shanghai 200240, China*
[2]*College of Physics and Communication Electronics, Jiangxi Normal University, Nanchang 330022, China*

Received November 8, 2011; accepted December 5, 2011; published online December 22, 2011

The ultrathin fiber taper fabricated by adiabatically stretching a heated single-mode optical fiber (SMF) is made in a C-shape bent to form a modal interferometer. The interference fringes due to the mode beating in the multimode taper waist are dependent on the bending radius. Under an optimized bending radius, a maximum 18 dB interference depth can be obtained. The influence of the fiber taper geometry on the interference fringes is discussed. The proposed modal interferometer has a high refractive index (RI) sensitivity of ~658 nm/RIU (refractive index unit) for RI = 1.333–1.353, which is expected to be useful for precision bio/chemical sensing applications.

Recently, optical fiber-taper-based Mach–Zehnder interferometer (MZI) RI sensors have attracted much interest because of their advantages such as small size, ease of fabrication, and low cost.[1–5] A number of fiber-taper-based MZI RI sensors have been developed by concatenating two or three single-mode fiber (SMF) tapers[1–3] or combining a fiber taper with a spot written in the fiber core using a femtosecond laser.[4] However, all these approaches have relatively low sensitivity for refractive index (RI) sensing. Most recently, Yang *et al.* have demonstrated an MZI based on a single S-tapered fiber,[5] which was fabricated by applying nonaxial pull while stretching the fused fiber. Since the diameter of the taper waist is quite large (about 65 μm), the MZI still has limited sensitivity (185 nm/RIU) for RI = 1.333–1.381 (i.e., the typical range of protein analytes). Besides, the quite high insertion loss (~10 dB) of the MZI degrades its potential applications.

In this paper, we propose a modal interferometer based on a C-shaped ultrathin optical fiber taper. It has unique features of low insertion loss (~4 dB), ultrathin taper waist (about several micrometers), high repeatability, and good reconfigurability. The optical ultrathin fiber taper was fabricated by adiabatically stretching a heated SMF in hydrogen flame, which consists of a uniform taper waist between a pair of transition regions. Locally bending the transition region of the fiber taper induces the coupling among multiple-order optical modes, which suffer different delays due to their different effective refractive indices in the middle taper waist. Consequently, it acts as an in-fiber modal interferometer, and the interference fringes can be optimized under a certain bending radius. The influences of the taper's diameter and length are also discussed. For RI sensing, the large evanescent field existing outside the ultrathin fiber taper can directly interact with the external materials.[6] A high sensitivity of about 658 nm/RIU was successfully realized for the range of RI = 1.333–1.353, which is approximately 4 times higher than that of the S-tapered fiber MZI RI sensor[5] and ~38 times that of the two-taper-based one.[1]

The fabrication of the optical fiber taper from an SMF was described in detail in refs. 7 and 8. The SMF with its jacket stripped was clipped and attached to two transition stages, which were separately controlled by two piezoelectric actuators. After the fiber was heated and softened in hydrogen flame, it was gradually pulled by the two moving translation stages under precise control. With a pulling speed of 0.165 mm/s, fiber tapers with different tapering profiles were obtained by changing the pulling time and adjusting the hydrogen flame position relative to the fiber. The tapering process is adiabatic.[9] The fiber taper can be divided into two zones: (1) the taper waist with a constant diameter d_0 and (2) the transition region with a diameter continuously varying from d_0 to 125 μm. Figure 1(a) shows the scanning electron microscopy (SEM) images of three fiber tapers with different d_0 varying from ~1.8 to ~3.7 μm. To configure a modal interferometer, the fiber taper was initially pulled straight and then gradually curved to form a symmetrically C-like shape. Figure 1(b) schematically illustrates the formation of the fiber-taper-based modal interferometer in the bending process. The bending process was monitored using an optical microscope. It is noted that the microbending occurs symmetrically in the two transition regions with an easily controllable microbending radius of R, and the taper waist is ultrathin from ~1.8 to ~3.7 μm remaining straight in the bending process. The maximum achievable bending curvature $1/R$ is ~1 mm^{-1}.

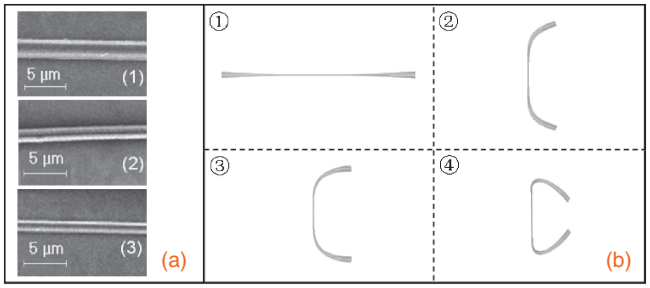

Fig. 1. (a) SEM images of the fiber taper with diameters of (1) $d_0 \approx 3.7$ μm, (2) $d_0 \approx 2.1$ μm, and (3) $d_0 \approx 1.8$ μm. (b) Formation of the fiber-taper-based C-shaped modal interferometer in a bending process.

A broadband light source is launched into one end of the fiber taper, and an optical spectrum analyzer (OSA) is connected to the other end for *in situ* characterization of its optical performance. The measured profile of the fiber taper, having the waist diameter $d_0 \approx 3.7$ μm, waist length $L_0 \approx 6$ mm, and bent transition region length $L_t \approx 3$ mm, is given in Fig. 2(a) together with the critical diameter corresponding to the bent transition region. Figure 2(b) shows the measured transmission spectra of the C-shaped taper-based modal

*E-mail address: lixinwan@sjtu.edu.cn

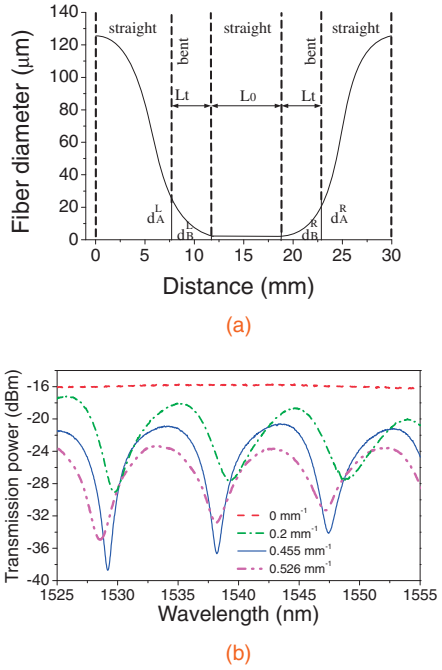

Fig. 2. (a) Measured profile of the microbent fiber taper having $d_0 \approx 3.7\,\mu\text{m}$, $L_0 \approx 6\,\text{mm}$, and $L_t \approx 3\,\text{mm}$ with d_A and d_B corresponding to the bent transition region. (b) Transmission spectra of the microbent taper-based modal interferometer under several bending curvatures ($1/R$).

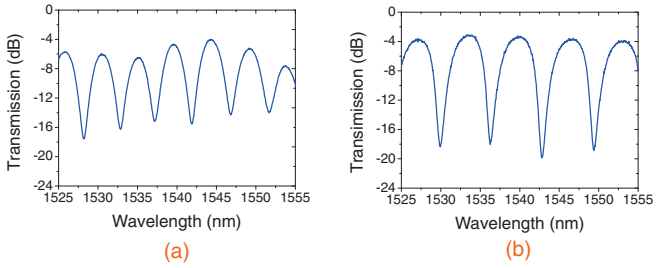

Fig. 3. Transmission spectra of microbent taper-based modal interferometers under optimized bending condition with (a) $d_0 \approx 3.7\,\mu\text{m}$, $L_0 \approx 12\,\text{mm}$, and (b) $d_0 \approx 2.1\,\mu\text{m}$, $L_0 \approx 6\,\text{mm}$.

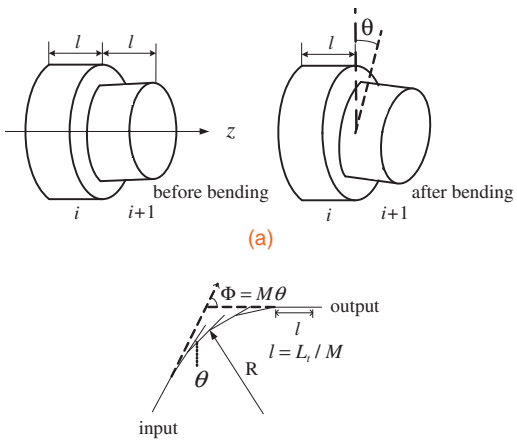

Fig. 4. (a) Two adjacent sections of a fiber taper before and after bending. (b) Geometry used for the theoretical analysis of the bending effect on the fiber taper.

interferometer under various bending curvatures $1/R$. The curve for $1/R = 0$ corresponds to the transmission spectrum of the straight optical taper before bending. When the optical taper is bent, a periodic interference pattern appears. The interference is strengthened when $1/R$ increases from 0 to about $0.455\,\text{mm}^{-1}$, and weakened when $1/R$ further increases to $0.526\,\text{mm}^{-1}$, which shows that there might be a certain bending curvature for optimizing the modal interference. One may also note from the figure that the transmission loss increases with decreasing bending radius.

Figures 3(a) and 3(b) show the transmission spectra of two other C-shaped taper-based modal interferometers with the same bending curvature of $1/R \approx 0.455\,\text{mm}^{-1}$ for waist parameters of $d_0 \approx 3.7\,\mu\text{m}$, $L_0 \approx 12\,\text{mm}$, and $d_0 \approx 2.1\,\mu\text{m}$, $L_0 \approx 6\,\text{mm}$, respectively. Compared with that in Fig. 2(b), the interference dips in Fig. 3 become sharper and narrower when d_0 decreases or L_0 increases.

To study the modal characteristics in the bent transition region, we assume the bent fiber taper as a sequence of straight segments of the same length l with an angle of θ[10,11] [see Fig. 4(a)]. The complex amplitude, $a_{pq}^{(i+1)}$, of the modes in the $(i+1)$th region is given by[11]

$$a_{pq}^{(i+1)} = \sum_{n=0}\sum_{m=1}\int_0^{\infty}\int_0^{2\pi} \psi_{nm}^{i} \exp(-j\beta_{nm}^{i} l^{i}) \times \exp(j\beta_{nm}^{i}\theta r\cos\phi)\psi_{pq}^{(i+1)*} r\,dr\,d\phi, \quad i = 1, 2, \qquad (1)$$

where β_{nm}^{i} is the propagation constant of the LP_{nm} mode in the ith region, l^{i} is the length of the ith region, ψ_{nm}^{i} is the modal field of the LP_{nm} mode in the ith region, and $\psi_{pq}^{(i+1)*}$ is the complex conjugate of the mode field of the LP_{pq} mode in the $(i+1)$th region.

We theoretically examine the local-mode power evolution along the bent fiber taper with $d_0 = 3.7\,\mu\text{m}$, $L_0 = 6\,\text{mm}$, and $L_t = 3\,\text{mm}$ at $\lambda = 1.555\,\mu\text{m}$ under various bending curvatures. Each bent transition region of the fiber taper was modeled with a value of $M = 100$ steps and each segment of the bent transition region has the same length (L_t/M). The uniform waist region has also been considered as a step of 6 mm width. The appropriate values of the angle θ in the bent transition region can be calculated from the modal as shown in Fig. 4(b). The first four modes LP_{01}, LP_{11}, LP_{21}, and LP_{02} have been used in the calculation and the results are shown in Fig. 5. When the bending curvature $1/R = 0$, there is no power transfer from the LP_{01} mode to other high-order modes. As the bending curvature increases, the high-order modes (LP_{11}, LP_{21}, and LP_{02}) are successively excited with their energy originated from the fundamental mode. In the central uniform taper waist region, the power remains almost constant for each mode. The coupling between the LP_{01} mode and LP_{11} mode, which essentially determines the interference extinction ratio, is strengthened as $1/R$ increases, but the bending loss increases accordingly. At a certain bending curvature (e.g., $0.455\,\text{mm}^{-1}$), the optimized status can be obtained since the interference extinction ratio almost reaches the maximum, whereas the transition loss is not too high.

The theoretical wavelength responses ranging from 1.525 to 1.555 μm for the same bent fiber taper under different

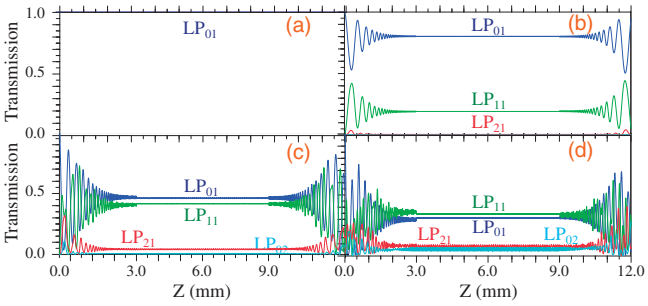

Fig. 5. LP_{nm} local-mode power longitudinal evolution of the microbent fiber taper with $d_0 = 3.7\,\mu m$ and $L_0 = 6\,mm$ under bending curvature $1/R$ being (a) 0, (b) 0.2, (c) 0.455, and (d) $0.526\,mm^{-1}$ at $\lambda = 1.555\,\mu m$.

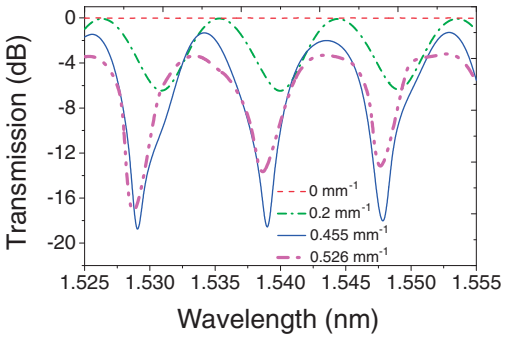

Fig. 6. Theoretical results of the transmission spectra of the microbent fiber taper with $d_0 = 3.7\,\mu m$, $L_0 = 6\,mm$, and $L_t = 3\,mm$ under different bending curvatures.

bending curvatures are shown in Fig. 6. Probably because of the fact that the fabricated fiber taper was not exactly symmetric, a small deviation exists between the theoretical approximation and experimental curves in Figs. 2(b) and 6.

The interference condition for two propagation modes in the bent fiber taper is given by

$$\Delta\beta L_0 = 2N\pi \quad (N = 1, 2, 3, \ldots), \tag{2}$$

where $\Delta\beta$ is the propagation constant difference between the two modes. The free spectral range (FSR) of the interference pattern is thus given by

$$\mathrm{FSR} \approx \frac{2\pi\lambda}{\Delta\beta L_0}, \tag{3}$$

where λ is the wavelength of light in vacuum. When the length is increased from $L_0 \approx 6$ to 12 mm for the same $d_0 \approx 3.7\,\mu m$, the FSR is decreased. When the taper waist diameter becomes smaller from $d_0 \approx 3.7$ to $2.1\,\mu m$ for the same $L_0 \approx 6\,mm$, the difference between the propagation constants becomes larger,[9] which also makes the FSR smaller [see Figs. 2(b) and 3].

Finally, we measured the transmission characteristics of the C-shaped taper with $d_0 \approx 3.7\,\mu m$ and $L_0 \approx 6\,mm$ for various surrounding refractive indices to study the potential RI sensing applications. The RI sensing measurement was performed at room temperature (25 °C) with a series of RI liquids. We prepared nine glycerol-water solutions with different volume concentrations (0.0, 1, 2, 3, 4, 5, 6, 7, and 8%). The corresponding n_{se} values (calculated from the Fresnel reflection using water as reference at 1550 nm at 25 °C) are 1.333, 1.3342, 1.3353, 1.3365, 1.3376, 1.3388, 1.340, 1.3412, and 1.3424, respectively. The interferometer was then mounted on a fiber holder and the sucrose solutions of different concentrations were placed from one of the bent taper transition regions using a dropper. Figure 7 shows the measured transmission spectra of the interferometer with various surrounding RIs. We found that the interference pattern is red-shifted (i.e., to the long-wavelength side) with a good linearity. The sensitivity is linearly fitted to be about 658 nm/RIU.

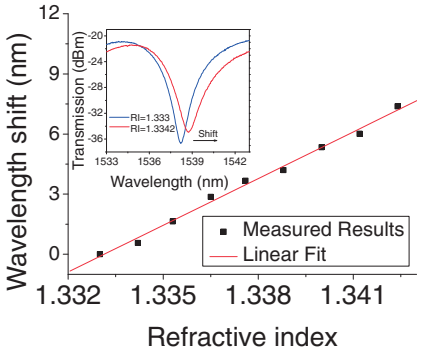

Fig. 7. Measured wavelength shifts of a certain transmission dip of the interferometer under various refractive indices.

In conclusion, we have experimentally and theoretically demonstrated a compact modal interferometer constructed by bending an ultrathin optical fiber taper. The dependence of the transmission interference spectrum on the taper geometrical parameters (bending curvature, waist diameter, and length) has been investigated. There is an optimized bending curvature to achieve a better interference pattern. The potential applications of the optimized interferometer as an RI sensor were also experimentally investigated and demonstrated. The interference fringe is shifted toward the long-wavelength side with an increasing surrounding RI and its sensitivity is about 658 nm/RIU. The proposed device is expected to be useful for high-precision bio/chemical sensing applications.

Acknowledgments This work was supported in part by the 973 program (ID2011CB301700), NSFC (60877012, 61007052, 61107041, 61127016), STCSM Project (10DJ1400402, 09JC1408100), and State Key Lab Projects (GKZD030004/09/15/20/21). The authors thank Professor Linjie Zhou for the valuable discussion and recommendation.

1) Z. Tian *et al.*: IEEE Photonics Technol. Lett. **20** (2008) 1387.
2) P. Lu *et al.*: Appl. Phys. Lett. **94** (2009) 131110.
3) D. Wu *et al.*: Appl. Opt. **50** (2011) 1548.
4) Z. Tian *et al.*: Opt. Lett. **33** (2008) 1105.
5) R. Yang *et al.*: to be published in Opt. Lett.
6) G. Brambilla *et al.*: Opt. Express **12** (2004) 2258.
7) Z. H. Hong *et al.*: Opt. Express **19** (2011) 3854.
8) J. P. Chen *et al.*: OECC, 2010, 8E2-1.
9) J. D. Love *et al.*: IEE Proc. **138** (1991) 343.
10) I. R. Matias *et al.*: Fiber Integrat. Opt. **22** (2003) 173.
11) P. M. Shankar *et al.*: J. Lightwave Technol. **9** (1991) 832.